A STUDY ON DRONE AND MATHEMATICAL MODELING OF DRONE OPERATING SYSTEM

Mainak Bhaumik[1], Rekha Rathore[2], Dr. Arun Kumar Lokhande [3], Dr. Laxmi Deepak Bhatlu[4], Jagdish Chahande[5], Basangoda Patil[6], Mahesh Pisal[7], Mahesh Patil[8], Anshuman Jha[9]*

*[1*5 6 7, 8]Assistant Professor in Mechanical Engineering Department in MGM's CET, Kamothe, New Mumbai, India -410209*

[2]Assistant Professor in Applied Science Department, in MGM's CET, Kamothe, New Mumbai, India -410209

[3]Professor in Chemical Engineering Department, and HOD in Mechanical Engineering Department, in MGM's CET, Kamothe, New Mumbai, India -410209

[9]Assistant Professor in Electrical Engineering Department, in MGM's CET, Kamothe, New Mumbai, India -410209

[1]mainak.bhaumik04@gmail.com

Abstract- A new trend of art of technology development with an advancement of drone operated vehicle is getting popularity for the ease of easier image processing, digester management, transportation, irrigation etc. It is a study, development and mathematical modeling of drone system. The study includes from fixed remote place the movement of drone on vertical, horizontal axis and on 360^0 rotation. This prior analysis of drone movement range is to have a prior clear idea with mathematical values before placing the drone for desired actual place of remote application with ease and accuracy. The human remote controlling and balancing of the drone movement has also been taken under consideration during the mathematical calculations.

Keywords: *Drone, Mathematical calculations, remote sensing,*

I. INTRODUCTION:

Now a days with the advancement of remote sensing technology, the drones are getting popularity and under study and experimentation in various fields to perform remote sensing operations. The drones are having popular versatile field of applications, such as in the photography, video making, digester management, agricultural fertilizer sprinkler application, in search and rescue applications at remote area, in delivering light affordable weight materials, in land area survey for 3-D mapping, in the field of security and safety surveillance etc. The battery capacity, battery backup, battery charging time and remote controller of the drone plays an important role to perform the drone for the purpose it is being manufactured and designed. The Fig. 1 illustrates the commercially available drone for the application of photography and security surveillance system. The Fig. 2 is about the commercial drone application in digester management of fire fighting system. In domestic, digester relief and engineering application for the transportation of materials the commercially available drone success has been illustrated in the Fig.3.

Fig. 1: Commercially available drone for photography and security surveillance.

Fig. 2: The Commercial drone in digester fire fighting system application.

II. PROBLEM DEFINITION:

The problem definition includes about the study of drone range determination and compatibility in performance to serve the designed range of the drone. A systematic mathematical calculation involves the drone load carrying capacity and carrying such designed load with self-load to perform the operation. The parameters considered in problem identification and definition under study and analysis involves self-weight and desired weight carrying capacity, drag and thrust forces acting and the influence of motion on the drone system. Here under analysis and study a four blades and rotors system drone has been taken under consideration and shown in Fig 4.

Fig. 3: In industrial material transportation purpose the involvement of commercially successful drone.

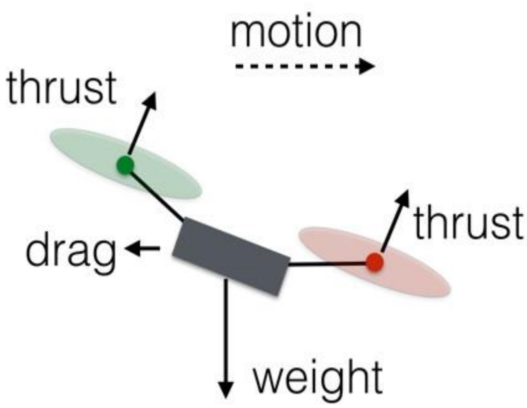

Fig. 4: Problem definition involvement parameters under study and analysis.

III. METHODOLOGY

The constructional methodology of the drone preparation involves preparation of aerofoil shape blades, brushless motors, drone body and material carrying device, rechargeable lithium ion battery remote control sensor. The proper design, assembly, balancing and experimentation by taking trial of drone involves the manual or automatic activity. In design and calculation part the detail calculation has been carried out by manual calculation. The drone movement analysis and basis detailed calculations can be analyzed by using commercially available software also. The Fig. 5 illustrates the involvement of major parts in drone preparation and assembly. This is an example of drone with camera for photography and video foot aging purpose for entertainment and security surveillance or for land survey and image collections for data analyzing.
In mathematical modeling the following parameters are taken under consideration, ξ for linear movement, η for angular movement, θ for pitch angle, Φ as rolling angle, ψ as yaw angle and q stands for vector of liner and angular position. These defined parameters are written in the form of matrix in the eq. 1. The linear and angular velocities are written in the eq. 2. The rotational phenomena, R of the drone has been shown in terms of equation in eq. 3. A schematic diagram of the factors in the calculations has been illustrated for better visualization and understanding in the Fig. 6. The table 1 tabulated the assumed values of the factors, parameters and constants.

$$\boldsymbol{\xi} = \begin{bmatrix} x \\ y \\ z \end{bmatrix}, \quad \boldsymbol{\eta} = \begin{bmatrix} \phi \\ \theta \\ \psi \end{bmatrix}, \quad \boldsymbol{q} = \begin{bmatrix} \boldsymbol{\xi} \\ \boldsymbol{\eta} \end{bmatrix}. \tag{1}$$

$$\boldsymbol{V}_B = \begin{bmatrix} v_{x,B} \\ v_{y,B} \\ v_{z,B} \end{bmatrix}, \quad \boldsymbol{\nu} = \begin{bmatrix} p \\ q \\ r \end{bmatrix}. \tag{2}$$

$$\boldsymbol{R} = \begin{bmatrix} C_\psi C_\theta & C_\psi S_\theta S_\phi - S_\psi C_\phi & C_\psi S_\theta C_\phi + S_\psi S_\phi \\ S_\psi C_\theta & S_\psi S_\theta S_\phi + C_\psi C_\phi & S_\psi S_\theta C_\phi - C_\psi S_\phi \\ -S_\theta & C_\theta S_\phi & C_\theta C_\phi \end{bmatrix}, \tag{3}$$

$$\begin{aligned} \dot{\boldsymbol{\eta}} = \boldsymbol{W}_\eta^{-1}\boldsymbol{\nu}, \quad & \begin{bmatrix} \dot\phi \\ \dot\theta \\ \dot\psi \end{bmatrix} = \begin{bmatrix} 1 & S_\phi T_\theta & C_\phi T_\theta \\ 0 & C_\phi & -S_\phi \\ 0 & S_\phi / C_\theta & C_\phi / C_\theta \end{bmatrix} \begin{bmatrix} p \\ q \\ r \end{bmatrix}, \\ \boldsymbol{\nu} = \boldsymbol{W}_\eta \dot{\boldsymbol{\eta}}, \quad & \begin{bmatrix} p \\ q \\ r \end{bmatrix} = \begin{bmatrix} 1 & 0 & -S_\theta \\ 0 & C_\phi & C_\theta S_\phi \\ 0 & -S_\phi & C_\theta C_\phi \end{bmatrix} \begin{bmatrix} \dot\phi \\ \dot\theta \\ \dot\psi \end{bmatrix}, \end{aligned} \tag{4}$$

I is for the inertia factor has been plotted in matrix is as shown in eq. 5. The angular force f_i is the factor of angular rotation ω_i which is shown in the eq. 6, while the k is a constant of proportionality, having value of consideration as mathematical value of 2.960 x 10^{-6}. The torque, τ produced by the rotor has also been equated in the eq. 6.

$$\boldsymbol{I} = \begin{bmatrix} I_{xx} & 0 & 0 \\ 0 & I_{yy} & 0 \\ 0 & 0 & I_{zz} \end{bmatrix}. \tag{5}$$

$$f_i = k\,\omega_i^2, \quad \tau_{M_i} = b\,\omega_i^2 + I_M\,\dot\omega_i, \tag{6}$$

Due to rotor and blade rotation the axial upward thrust, T generated can be calculated by using the eq. 7. In the same upward direction the torque, τ_B produced has been written in terms of matrix form in the eq. 8.

$$T = \sum_{i=1}^{4} f_i = k \sum_{i=1}^{4} \omega_i^2, \quad \boldsymbol{T}^B = \begin{bmatrix} 0 \\ 0 \\ T \end{bmatrix}, \tag{7}$$

$$\boldsymbol{\tau}_B = \begin{bmatrix} \tau_\phi \\ \tau_\theta \\ \tau_\psi \end{bmatrix} = \begin{bmatrix} l\,k\,(-\omega_2^2 + \omega_4^2) \\ l\,k\,(-\omega_1^2 + \omega_3^2) \\ \sum_{i=1}^{4} \tau_{M_i} \end{bmatrix}, \tag{8}$$

When the blade starts rotating, the centrifugal forces come in picture and also the momentum phenomena are as shown in the eq. 9. The term ($m\ V_B$), momentum and $v\ x\ (m\ V_B)$ is centrifugal force factor. The gravity term considered as $R^T G$. Considered T_B as total value of thrust parameter.

$$m\dot{\boldsymbol{V}}_B + \boldsymbol{\nu} \times (m\,\boldsymbol{V}_B) = \boldsymbol{R}^{\mathrm{T}}\boldsymbol{G} + \boldsymbol{T}_B. \qquad (9)$$

The combined magnitude of gravity and thrust is as shown in the eq. 10. It contributes to understand the acceleration phenomena.

$$m\ddot{\boldsymbol{\xi}} = \boldsymbol{G} + \boldsymbol{R}\boldsymbol{T}_B,$$

$$\begin{bmatrix} \ddot{x} \\ \ddot{y} \\ \ddot{z} \end{bmatrix} = -g \begin{bmatrix} 0 \\ 0 \\ 1 \end{bmatrix} + \frac{T}{m} \begin{bmatrix} C_\psi S_\theta C_\phi + S_\psi S_\phi \\ S_\psi S_\theta C_\phi - C_\psi S_\phi \\ C_\theta C_\phi \end{bmatrix}. \qquad (10)$$

The influence of angular acceleration on the drone body frame is *Iv*

$$\boldsymbol{I}\dot{\boldsymbol{\nu}} + \boldsymbol{\nu} \times (\boldsymbol{I}\boldsymbol{\nu}) + \boldsymbol{\Gamma} = \boldsymbol{\tau},$$

$$\dot{\boldsymbol{\nu}} = \boldsymbol{I}^{-1}\left(-\begin{bmatrix} p \\ q \\ r \end{bmatrix} \times \begin{bmatrix} I_{xx}\,p \\ I_{yy}\,q \\ I_{zz}\,r \end{bmatrix} - I_r \begin{bmatrix} p \\ q \\ r \end{bmatrix} \times \begin{bmatrix} 0 \\ 0 \\ 1 \end{bmatrix} \omega_\Gamma + \boldsymbol{\tau} \right), \qquad (11)$$

$$\begin{bmatrix} \dot{p} \\ \dot{q} \\ \dot{r} \end{bmatrix} = \begin{bmatrix} (I_{yy} - I_{zz})\,q\,r/I_{xx} \\ (I_{zz} - I_{xx})\,p\,r/I_{yy} \\ (I_{xx} - I_{yy})\,p\,q/I_{zz} \end{bmatrix} - I_r \begin{bmatrix} q/I_{xx} \\ -p/I_{yy} \\ 0 \end{bmatrix} \omega_\Gamma + \begin{bmatrix} \tau_\phi/I_{xx} \\ \tau_\theta/I_{yy} \\ \tau_\psi/I_{zz} \end{bmatrix},$$

The body force acceleration, W^{-1}_η with respect to time derivative is as shown in eq. 12.

$$\ddot{\eta} = \frac{\mathrm{d}}{\mathrm{d}t}\left(W_\eta^{-1}\nu\right) = \frac{\mathrm{d}}{\mathrm{d}t}\left(W_\eta^{-1}\right)\nu + W_\eta^{-1}\dot{\nu}$$

$$= \begin{bmatrix} 0 & \dot{\phi}C_\phi T_\theta + \dot{\theta}S_\phi/C_\theta^2 & -\dot{\phi}S_\phi C_\theta + \dot{\theta}C_\phi/C_\theta^2 \\ 0 & -\dot{\phi}S_\phi & -\dot{\phi}C_\phi \\ 0 & \dot{\phi}C_\phi/C_\theta + \dot{\phi}S_\phi T_\theta/C_\theta & -\dot{\phi}S_\phi/C_\theta + \dot{\theta}C_\phi T_\theta/C_\theta \end{bmatrix} \nu + W_\eta^{-1}\dot{\nu}. \qquad (12)$$

The Lagrangian term, *L* of energy is the summation of translational energy *Etrans* and rotational energy *Erot* . It has been shown in the eq. 13 and 14.

$$\begin{aligned} \mathcal{L}(\boldsymbol{q}, \dot{\boldsymbol{q}}) &= E_{trans} + E_{rot} - E_{pot} \\ &= (m/2)\,\dot{\boldsymbol{\xi}}^{\mathrm{T}}\dot{\boldsymbol{\xi}} + (1/2)\,\boldsymbol{\nu}^{\mathrm{T}}\boldsymbol{I}\,\boldsymbol{\nu} - mgz. \end{aligned} \qquad (13)$$

$$\begin{bmatrix} \boldsymbol{f} \\ \boldsymbol{\tau} \end{bmatrix} = \frac{\mathrm{d}}{\mathrm{d}t}\left(\frac{\partial \mathcal{L}}{\partial \dot{\boldsymbol{q}}}\right) - \frac{\partial \mathcal{L}}{\partial \boldsymbol{q}}. \qquad (14)$$

The external linear force, *f* is the blade rotor thrust. This has been expressed by using eq. 15.
Jacobian equation, $J(\eta)$ is expressed in eq. 15 and 16.

$$\boldsymbol{f} = \boldsymbol{R}\boldsymbol{T}_B = m\ddot{\boldsymbol{\xi}} + mg \begin{bmatrix} 0 \\ 0 \\ 1 \end{bmatrix}, \qquad (15)$$

$$\boldsymbol{J}(\boldsymbol{\eta}) = \boldsymbol{J} = \boldsymbol{W}_\eta^{\mathrm{T}}\,\boldsymbol{I}\,\boldsymbol{W}_\eta,$$

$$= \begin{bmatrix} I_{xx} & 0 & -I_{xx}S_\theta \\ 0 & I_{yy}C_\phi^2 + I_{zz}S_\phi^2 & (I_{yy} - I_{zz})\,C_\phi S_\phi C_\theta \\ -I_{xx}S_\theta & (I_{yy} - I_{zz})\,C_\phi S_\phi C_\theta & I_{xx}S_\theta^2 + I_{yy}S_\phi^2 C_\theta^2 + I_{zz}C_\phi^2 C_\theta^2 \end{bmatrix}. \qquad (16)$$

The rotational inertial force *Erot* is also expressed in the eq. 17.

$$E_{rot} = (1/2)\,\boldsymbol{\nu}^{\mathrm{T}}\,\boldsymbol{I}\,\boldsymbol{\nu} = (1/2)\,\dot{\boldsymbol{\eta}}^{\mathrm{T}}\,\boldsymbol{J}\,\dot{\boldsymbol{\eta}}. \qquad (17)$$

The combined Euler-Lagrange equations are as expressed in eq. 18 and eq. 19.

$$\boldsymbol{\tau} = \boldsymbol{\tau}_B = \boldsymbol{J}\,\ddot{\boldsymbol{\eta}} + \frac{\mathrm{d}}{\mathrm{d}t}(\boldsymbol{J})\,\dot{\boldsymbol{\eta}} - \frac{1}{2}\frac{\partial}{\partial \boldsymbol{\eta}}\left(\dot{\boldsymbol{\eta}}^{\mathrm{T}}\,\boldsymbol{J}\,\dot{\boldsymbol{\eta}}\right) = \boldsymbol{J}\,\ddot{\boldsymbol{\eta}} + \boldsymbol{C}(\boldsymbol{\eta}, \dot{\boldsymbol{\eta}})\,\dot{\boldsymbol{\eta}}. \qquad (18)$$

In the matrix form Coriolis equations, $C(\eta,\eta^{\cdot})$ of gyroscopic and centrifugal factor is as expressed in the eq. 19.

$$\boldsymbol{C}(\boldsymbol{\eta},\dot{\boldsymbol{\eta}}) = \begin{bmatrix} C_{11} & C_{12} & C_{13} \\ C_{21} & C_{22} & C_{23} \\ C_{31} & C_{32} & C_{33} \end{bmatrix},$$

$$\begin{aligned}
C_{11} &= 0 \\
C_{12} &= (I_{yy}-I_{zz})(\dot{\theta}C_\phi S_\phi + \dot{\psi}S_\phi^2 C_\theta) + (I_{zz}-I_{yy})\dot{\psi}C_\phi^2 C_\theta - I_{xx}\dot{\psi}C_\theta \\
C_{13} &= (I_{zz}-I_{yy})\dot{\psi}C_\phi S_\phi C_\theta^2 \\
C_{21} &= (I_{zz}-I_{yy})(\dot{\theta}C_\phi S_\phi + \dot{\psi}S_\phi C_\theta) + (I_{yy}-I_{zz})\dot{\psi}C_\phi^2 C_\theta + I_{xx}\dot{\psi}C_\theta \\
C_{22} &= (I_{zz}-I_{yy})\dot{\phi}C_\phi S_\phi \\
C_{23} &= -I_{xx}\dot{\psi}S_\theta C_\theta + I_{yy}\dot{\psi}S_\phi^2 S_\theta C_\theta + I_{zz}\dot{\psi}C_\phi^2 S_\theta C_\theta \\
C_{31} &= (I_{yy}-I_{zz})\dot{\psi}C_\theta^2 S_\phi C_\phi - I_{xx}\dot{\theta}C_\theta \\
C_{32} &= (I_{zz}-I_{yy})(\dot{\theta}C_\phi S_\phi S_\theta + \dot{\phi}S_\phi^2 C_\theta) + (I_{yy}-I_{zz})\dot{\phi}C_\phi^2 C_\theta \\
&\quad + I_{xx}\dot{\psi}S_\theta C_\theta - I_{yy}\dot{\psi}S_\phi^2 S_\theta C_\theta - I_{zz}\dot{\psi}C_\phi^2 S_\theta C_\theta \\
C_{33} &= (I_{yy}-I_{zz})\dot{\phi}C_\phi S_\phi C_\theta^2 - I_{yy}\dot{\theta}S_\phi^2 C_\theta S_\theta - I_{zz}\dot{\theta}C_\phi^2 C_\theta S_\theta + I_{xx}\dot{\theta}C_\theta S_\theta.
\end{aligned} \tag{19}$$

The equivalent equation of angular movement, η is as expressed in the eq. 20.

$$\ddot{\boldsymbol{\eta}} = \boldsymbol{J}^{-1}\left(\boldsymbol{\tau}_B - \boldsymbol{C}(\boldsymbol{\eta},\dot{\boldsymbol{\eta}})\,\dot{\boldsymbol{\eta}}\right). \tag{20}$$

The aerodynamic effect with diagonal co-efficient are as expressed in the eq. 21.

$$\begin{bmatrix} \ddot{x} \\ \ddot{y} \\ \ddot{z} \end{bmatrix} = -g\begin{bmatrix} 0 \\ 0 \\ 1 \end{bmatrix} + \frac{T}{m}\begin{bmatrix} C_\psi S_\theta C_\phi + S_\psi S_\phi \\ S_\psi S_\theta C_\phi - C_\psi S_\phi \\ C_\theta C_\phi \end{bmatrix} - \frac{1}{m}\begin{bmatrix} A_x & 0 & 0 \\ 0 & A_y & 0 \\ 0 & 0 & A_z \end{bmatrix}\begin{bmatrix} \dot{x} \\ \dot{y} \\ \dot{z} \end{bmatrix}, \tag{21}$$

Fig.5: An illustration of major components requirements in camera loaded drone assembly system.

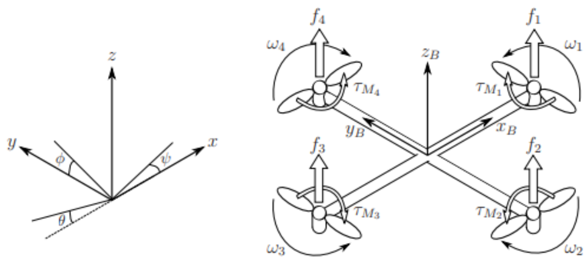

Fig.6: Schematic diagram of the values and factors of the terms in drone modeling and calculations.

Table 1: Values for calculations.

Parameter	Value	Unit	Parameter	Value	Unit
g	9.81	m/s^2	I_{xx}	$4.856 \cdot 10^{-3}$	kg m^2
m	0.468	kg	I_{yy}	$4.856 \cdot 10^{-3}$	kg m^2
l	0.225	m	I_{zz}	$8.801 \cdot 10^{-3}$	kg m^2
k	$2.980 \cdot 10^{-6}$		A_x	0.25	kg/s
b	$1.140 \cdot 10^{-7}$		A_y	0.25	kg/s
I_M	$3.357 \cdot 10^{-5}$	kg m^2	A_z	0.25	kg/s

IV. RESULTS AND DISCUSSIONS:

Considering the equations and substituting the considered parameter values the calculations has been performed. The various iterations are being plotted in terms of graphs. The Fig. 7 illustrates the time transient calculations of rolling angle Φ, pitch angle θ and yaw angle ψ. One more time transient analysis with respect to input angular speed (ωi) is as shown in the Fig. 8. The Fig. 9 is about the time transient v/s drone moving position in different axis of movement.

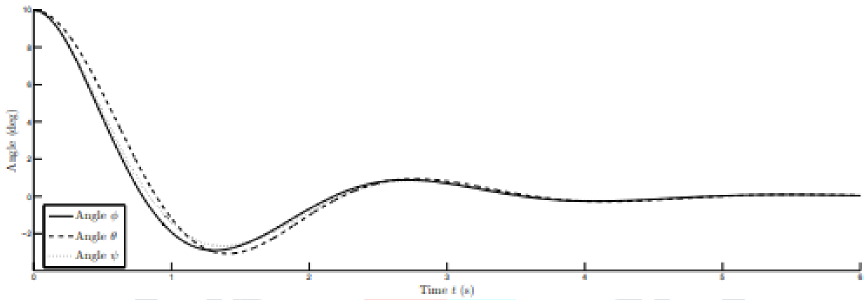

Fig. 7: Time transient v/s Angle of motion.

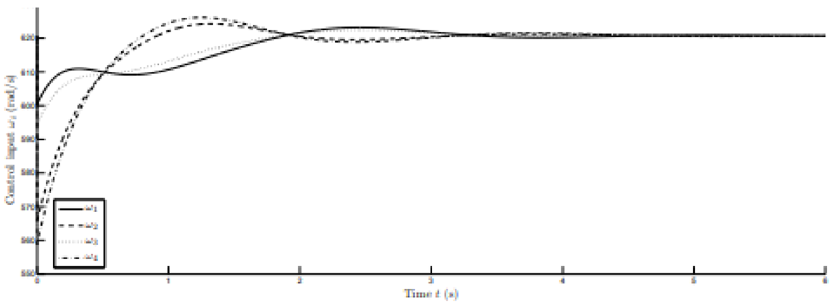

Fig. 8: Time transient v/s input control angular speed (ωi).

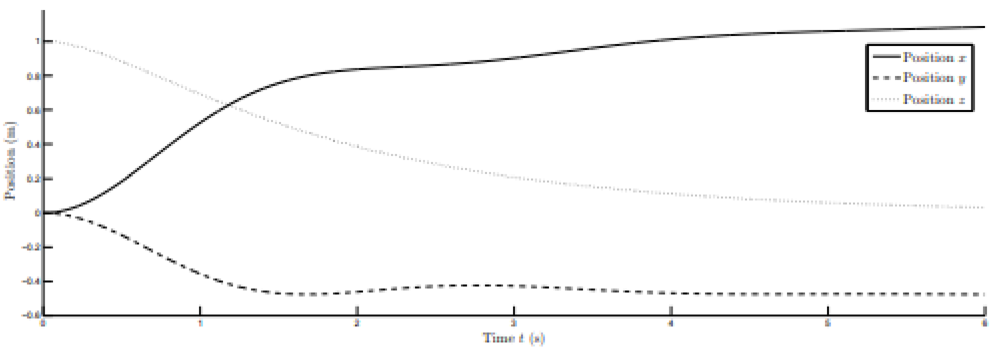

Fig. 9: Time transient v/s drone movement position in different axis.

V. CONCLUSION

After a study and analysis it can be derived a conclusion that in drone designing prior mathematical calculations to be carried out to avoid the failure of the drone and to know the range and prior performance estimation of the drone performance. The considered parameters to be written in the form of matrixes and to be solved and analyzed the data and obtained values of range, force, velocity vectors, momentum etc. From the various plots of time transient v/s drone linear movement, angular position and input angular movement it can be concluded for the same time transient parameters of upto six seconds that the horizontal x directional movement is quite rapid. For the considered parameters the drone can perform the operation of movement within six seconds upto a distance of one meter.

REFERENCES

[1] Can Huang, Chenghua Xu, Bin Wang, Xiaodong Hu, Junjie Li, Jiangying Liu, Jie Liu, Chenxi Li. 2018. High production of syngas from catalytic steam reforming of biomass glycerol in the presence of methane. Biomass and Bioenergy. 119: 173-178.

[2] Youngliang Xie, Xujiang Wang, Haiquan Bi, Yanping Yuan, Jinhua Wang, Zuohua Huang. 2018. A comprehensive review on laminar spherically premixed flame propogation of syngas. Fuel Processing Technology, 181 97 – 114.

[3] Susanna Maisano, Francesco Urbani, Francesco Cipit,Fabrizio Freni, Vitaliano Chiodo. 2018. Syngas production by BFB Gasification : Experimental comparison of different biomasses. Hydrogen Energy, 1.

[4] Mohd Nasir Nor Shahirah , Jolius Gimbun, Su Shiung Lam, Yun Hau Ng, Chin Kui Cheng. 2019. Synthesis and characterization of a La- Ni / α – Al2O3 catalysy and its use in pryoloysis of glycerol to syngas. Renewal Energy, 132:1389 – 1401.

[5] Gang Luo, Yuhang Jing, Yujin Lin, Shicheng Zhang, Dong An, (2018). A novel concept for syngas biomethanation by two-stage process: Focusing on the selective conversion of syngas to acetate. Science of the Total Environment, 645: 1194 – 1200.

[6] Ftwi Yohaness Hagos, A. Rashid A. Aziz, Shaharin A. Sulaiman, Rizalman Mamat, 2018. Engine speed and air-fuel ratio effect on the combustion of methane augmented hydrogen rich syngas in DI SI engine. Hydrogen Energy, 1-10.

[7] Kai Li, Jing-Lin Liu, Xiao-Song Li, Hao-Yu Lian, Xiaobing Zhu, Annemie Bogaerts, Ai-Min Zhu. 2018. Novel power to syngas concept for plasma catalytic reforming coupled with water electrolysis. Chemical Energy Journal, 353: 297-304.

[8] Willian C_ezar Nadaleti. 2019. Utilization of residues from rice parboiling industries in southern Brazil for Biogas and hydrogen-syngas generation : Heat, electricity and energy planning. Renewal Energy, 131: 55-72.

[9] Abel F.G. Neto, Francisco C. Marques, Adriana T. Amador, Amanda D.S. Ferreira, Antonio M.J.C. Neto. 2019. DFT and canonical ensemble investigations on the thermodynamic properties of Syngas and natural gas/Syngas mixtures. Renewable Energy, 130: 495-509.

[10] Xiao Sun, Hasan K. Atiyeh, Ajay Kumar, Hailin Zhang, Ralph S. Tanner. 2018, “Biochar enhanced ethanol and butanol production by Clostridium carboxidivorans from syngas. Bioresource Technology, 265: 128-138.

[11] Lu-Qing Wang, Hong-Hao Ma, Zhao-Wu Shen,Yang-Fan Cheng, Dai-Guo Chen. 2018. Detonation behaviors of syngas-oxygen in round and square tubes. Hydrogen Energy, 1-12.

[12] Zhen Xu, Ming Jia, Yaopeng Li, Yachao Chang, Guangfu Xu, Leilei Xuc, Xingcai Lu. 2018. Computational optimization of fuel supply, syngas composition, and intake conditions for a syngas/diesel RCCI engine. Fuel, vol. 234: 120-134.